New Simple Large Depth of Field Fringe Projection Profilometry System Using Laser Projector

H. A. Ali[a]*, M. A. Amer[a]. A. A. Omara[b]

[a]Engineering & Surface Metrology Laboratory, National Institute of Standards (NIS)

[b]Physics Department, Faculty of Science, Al-Azhar University

*Corresponding Author E-mail: hanem.abdraboh@nis.sci.eg

Article Type: Research article.
Received on 13 July 2021, Accepted on 22 September 2021

Abstract

Fringe Projection Profilometry (FPP) is a widely used non-contact technique for 3D measurements in different fields such as reserve engineering, quality assurance and security systems. Traditional FPP systems suffer from many problems i.e., limited working distance and large phase error. These problems exist due to the limited depth of field of the optical element of the systems components and nonlinear gamma response. This paper introduces large depth of field FPP system utilizing focus-free laser projector. Nonlinear gamma effect of red, blue, and green channels is studied, and phase error is calculated for each. Also, the focus-free projection of the projector at different distances up to 1725 mm is studied. Large depth of the field and the working distance of the system equal to 300 mm within the distance from 800 to 500 mm were proved with improved phase error. The large depth of field and working distance of the system are demonstrated by phase map calculation of cylindrical surface at four different distances equal to 800, 700, 600 and 500 mm.

Keywords: Fringe Projection Profilometry (FPP); Laser projector; Depth of field (DOF).

1. Introduction

In the last two decades' fringe projection profilometry (FPP) is widely used in diverse fields due to its flexibility, accuracy, and speed [1-7]. In (FPP) system fringe patterns with certain structure are projected onto object surface. These fringes will be deformed due to the object height distribution. The image of deformed fringes is captured by a CCD camera, then analyzed by one of analysis technique such as Fourier transform, wavelet transform and phase shifting technique to get the phase map. A suitable phase unwrapping algorithm is used to obtain the absolute phase map. Finally, the system is calibrated to transform from the phase map to real world coordinate [8-9].

Fringe patterns can be produced by different methods using optical elements such as commercial beam splitting cube [10], diffractive optical element interferometer [11], simple fibre optic coupler to form a Young's double pinhole interferometer [12]. It can also be produced by the interference of two laser beams, which are frequency modulated by a pair of acousto-optic modulators [13], Circular Ronchi grating with Kohler illumination system [14], or can be generated digitally using computer software and projecting it by projecting devices like Liquid Crystal Display (LCD) projectors [15], Digital Light Processor (DLP) projectors

[16-17]. Both of DLP and LCD projectors use lenses for projecting focused fringes. When sinusoidal fringe patterns are used, if the projector is defocused, it causes blurring of the projected patterns despite keeping phase unchanged and lowering signal to noise ratio [18].
As the defocusing level increases the phase error increases dominated by single frequency component due to the imbalance of the fringe image [19]. As a result, traditional FPP systems suffer from two main problems which are limited working distance and large phase error. These problems exist due to the limited depth of field of the optical element of the systems components and nonlinear gamma response. This paper introduces a new simple large depth of field FPP system using laser projector. It is a new type of projectors where it introduces a focus-free image projection, i.e., the images are always focused, even when projected at different distance opening the field to increase the working range of (FPP) system. Nonlinear gamma effect of the system is studied as well as proving the large depth of field of the system.
As a practical example, a cylindrical object is imaged at different distances to demonstrate the large depth of field of the system.

2. Phase shifting algorithm

Fringe analysis plays an important role in FPP system. It affects the performance, resolution, and accuracy of measurement [4]. Many different analysis techniques were developed for retrieving the phase map such as Fourier transform [20-22], Windowed Fourier transform [22-23], wavelet transform [23-24] and Phase shifting algorithm [4,25]. Phase shifting method is accurate, robust, can achieve pixel-wise phase measurement with high resolution and accuracy and robust to ambient illumination and varying surface reflectivity [26]. At least three fringe images with a certain phase shift are required to get the phase map. Let us consider three wave-fronts shifted by $2\pi/3$ with intensities

$$I_1(x,y,t) = I'(x,y) + I''(x,y)\cos\{\varphi(x,y) - 2\pi/3\} \quad (1)$$
$$I_2(x,y,t) = I'(x,y) + I''(x,y)\cos\{\varphi(x,y)\} \quad (2)$$
$$I_3(x,y,t) = I'(x,y) + I''(x,y)\cos\{\varphi(x,y) + 2\pi/3\} \quad (3)$$

where $I'(x,y)$ is the average intensity, $I''(x,y)$ is the intensity modulation and $\varphi(x,y)$ is the phase needed to be known. By solving the three equations the extracted phase will be

$$\varphi(x,y) = \tan^{-1}\left[\frac{\sqrt{3}\,(I_1 - I_3)}{(2I_2 - I_1 - I_3)}\right] \quad (4)$$

The obtained phase values are from 0 to 2π, so a suitable phase unwrapping algorithm is used to get the continuous phase map.

3. Research Methodology

3.1. Test system

This study was performed using FPP system consists of laser mobile pico projector manufactured by Sony, Model MP-CL1A, Mobile projector. This device emits class 3R laser with wavelength from 445 nm to 639 nm and beam divergence 4.5 mrad. Colour CCD camera manufactured by Edmund optics, Model EO-18112, attached with a lens manufactured by Edmund optics model FL 33-302 and a computer manufactured by Dell, model latitude 5580 are used to perform the experimental work of this study. Image of the system is shown in Fig. 1. Fig. 2 illustrates a schematic diagram of the system. The optical axis of the projector (P) and CCD camera (C) are separated by distance (D). Both of P and C are placed away from reference surface (R) at normal distance (L). A light beam with certain phase is projected on object surface at point A will be imaged at certain pixel of the camera. If an object with height

(h) is placed between R and (C, P) the light beam will hit the object surface at point B. For the projector point, A and B have the same phase. For the camera, point B and A' have the same phase. From the geometry of the system, the object height h could be given by the following equation

$$h = \frac{1}{\left(\frac{D}{A'A}\right)+1} \qquad (5)$$

where A'A is the phase shift caused by the object height. The object height h could be represented as a function of phase shift

$$h = f(A'A)$$

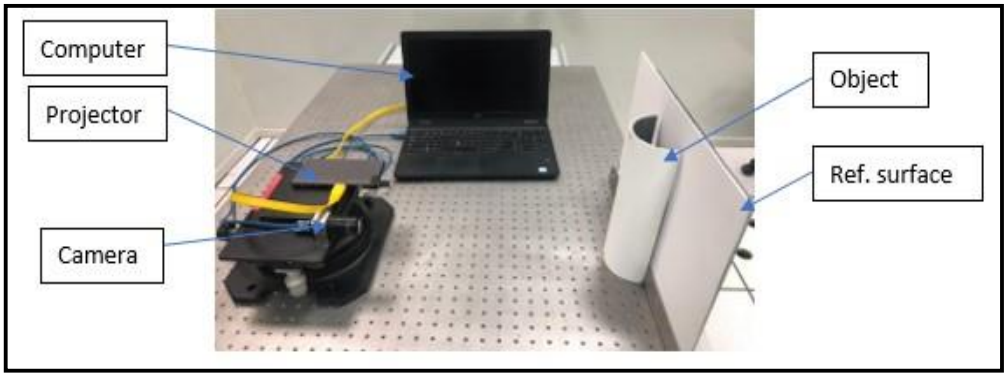

Fig. 1. Image of FPP system.

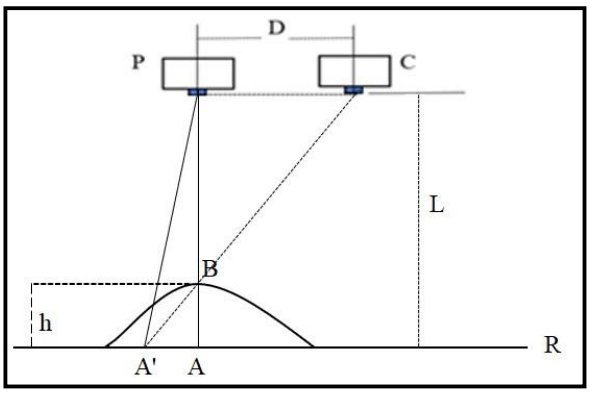

Fig. 2. A schematic diagram of used FPP system.

3.2. Nonlinear gamma effect

It is known that CCD cameras and digital projectors represent colours by intensities ranging between 0 and 255. Also, they behave nonlinear response to the input or captured intensities. This behavior is known as nonlinear gamma effect. Nonlinear gamma effect is studied for all three colours channels, red, green, and blue, to find the one that has the smallest phase error.
Nonlinear gamma effect is studied using a set of gray scale images having different intensities (Io) varying from 20 to 220 with regular step 10. The projected images are captured by the camera. Small area (10 x10 pixels) at the center of the image is analyzed and the intensity average value is considered as the output intensity (I). Nonlinear gamma effect curve is obtained as a relation between Io and I.

3.3. Phase error

To predict the phase error due to nonlinear gamma effect of red, green, and blue channels, three ideal sinusoidal waves shifted by $2\pi/3$ is generated with fringe width 250 pixels. This large fringe width is chosen to better show the effect of nonlinear gamma response of the system on the sinusoidal waves and unwrapped phase. These waves are distorted according to nonlinear gamma effect curve of each channel. Equation (4) is applied to obtain ideal (φ_i) and distorted (φ_d) phase maps for red, green, and blue channels, then phase maps are unwrapped to remove 2π jumps. Phase error was calculated by subtracting distorted and ideal phase map [27].

To determine actual phase error of red, green, and blue channels, three sinusoidal fringe patterns shifted by $2\pi/3$ with fringe width 30 pixels of each colour are projected on a reference surface. Fig. 3 illustrate the captured images of each colour. Phase maps were retrieved using Equation 4, then unwrapped to remove 2π discontinuities. Slope of unwrapped phase was removed to show phase error [19].

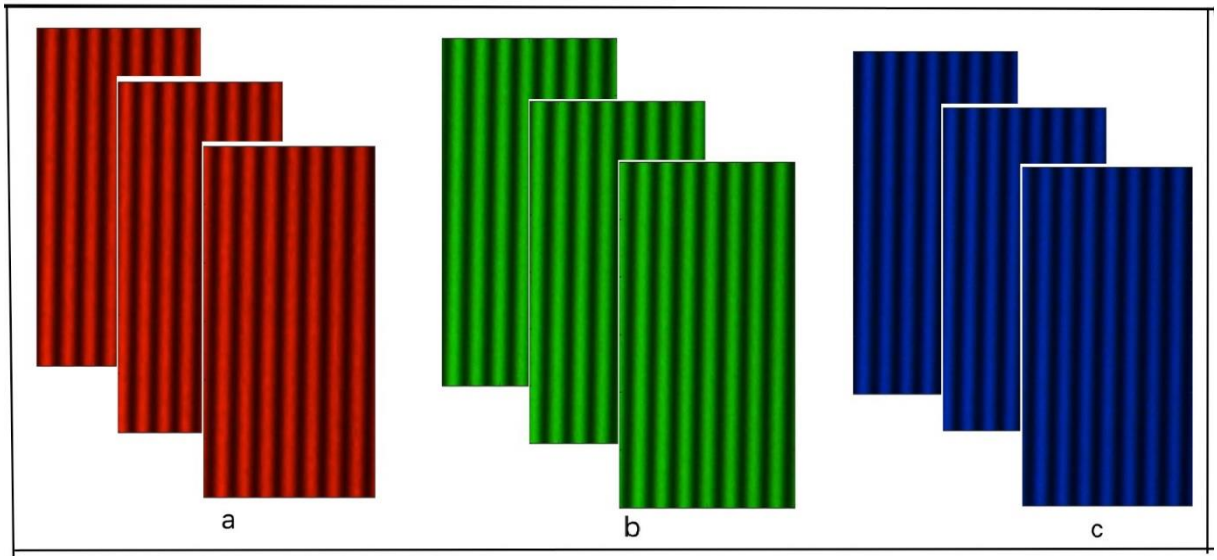

Fig. 3. Images of projected sinusoidal fringes of red colour (a), green colour (b), and blue colour (c).

3.4. Free-focus projection and depth of field (DOF).

In this study, a new type of projectors is used. It is a laser projector has the advantage of focus-free projection. This behavior is proved by projecting green binary pattern coded using matlab 2018a on a reference surface placed at different distances 500, 1000, 1500 and 1725 mm. At each distance, the camera parameters such as (lens aperture, gain, exposure time) need to be changed to get sharp and clear image of the binary pattern as shown in Fig. 4 (a, b, c, and d). The green channel of the image is separated for farther analysis as shown in Fig. 4 (e, f, g and h). The actual phase error at each distance is calculated as mentioned in section 3-3.

To Realize the large (DOF) of the system, green binary patterns are projected on the flat reference surface placed at 800 mm away from the projector. This distance is changed by moving the reference surface from 800 mm to 500 mm in regular steps equal to 100 mm towards the camera and projector. The camera parameters were fixed to certain values at all distances and the aperture of lens is reduced to increase (DOF) of the camera [19]. Green channel of the image is separated for using it in farther analyses as shown in Fig. 5 (a, b, c, and d). Since sinusoidal fringes are the most type of fringes that used to calculate the phase map, it is useful to study how they behave within the supposed (DOF). This is done by projecting green

sinusoidal fringes at 800, 700, 600, and 500 mm. Again, green channel of the image is separated to be used in farther analysis as shown in Fig. 5 (e, f, g, and h). Finally, the actual phase error at each distance is calculated as mentioned in section 3-3.

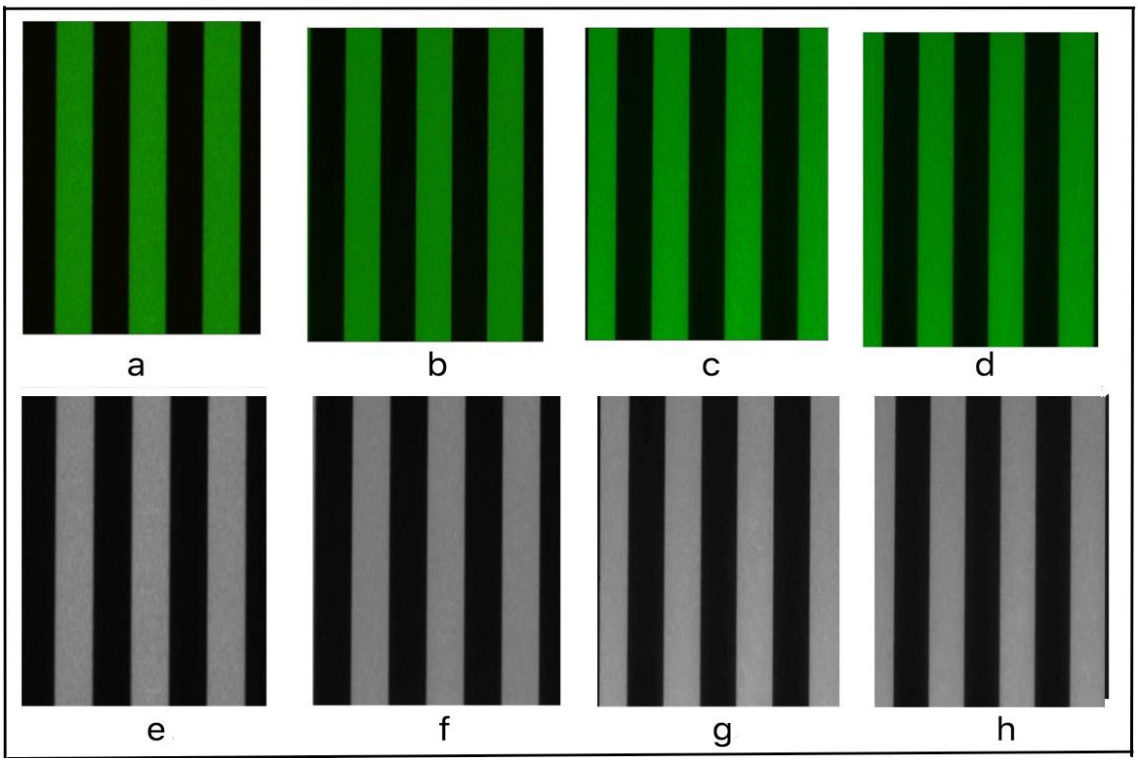

Fig. 4. Images of binary pattern at 500 mm (a), 1000 mm (b), 1500 mm (c) and 1725 mm (d) respectively. Image of green channel at 500 mm (e), 1000 mm (f), 1500 mm (g) and 1725 mm (h) respectively.

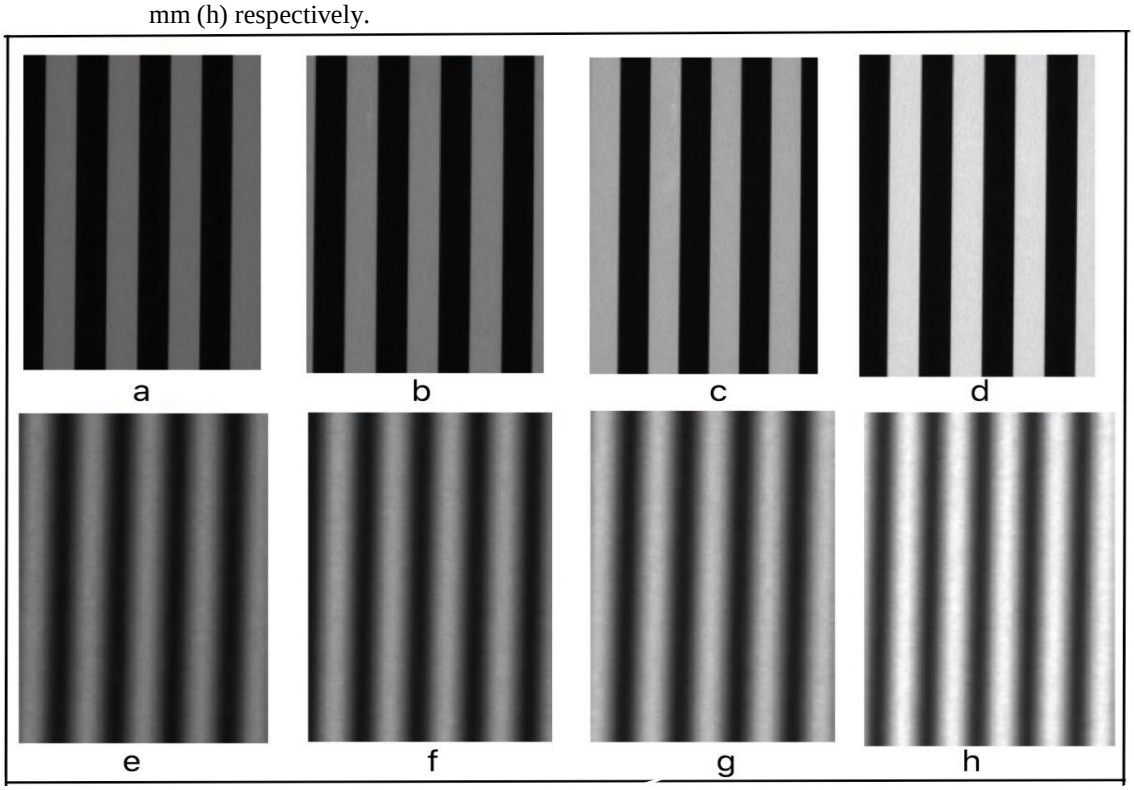

Fig. 5. Images of binary pattern at 800 mm (a), 700 mm (b), 600 mm (c) and 500 mm (d) respectively. Images of sinusoidal pattern at 800 mm (e), 700 mm (f), 600 mm (g) and 500 mm (h) respectively.

3.5 Practical example

As a practical example to ensure the efficiency of the system to have large depth of field, a cylindrical object is imaged at four different positions (800, 700, 600 and 500) mm using three sinusoidal fringe patterns shifted by $2\pi/3$. The camera parameters are kept constant at all distances. Wrapped Phase is calculated then unwrapped to get continuous phase map at each position for reference surface and the object. The phase shift due to the object existence is calculated by subtracting the object unwrapped phase map and the reference unwrapped phase map at each distance.

4. Results and Discussion

4.1. Nonlinear gamma effect

Fig. 6 shows the nonlinear gamma effect curve of red, green, and blue channels. It is found that the relation between (Io) and (I) is represented by a polynomial of 3rd order.

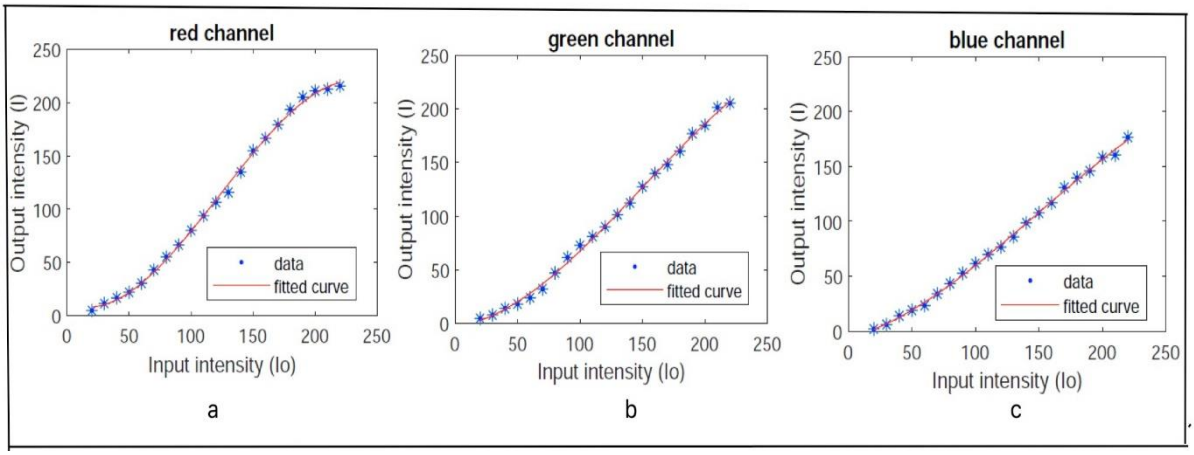

Fig. 6. Nonlinear gamma effect curves for red (a), green (b), and blue (c) channels respectively.

4.2. Phase error

Ideal and distorted sinusoidal wave of red, green, and blue channels according to nonlinear gamma effect curve are shown in Fig. 7 and the unwrapped phase map is illustrated in Fig. 8. Fig. 9 shows the phase error using nonlinear gamma effect curve of red, green, and blue channels. It is found that the red channel has the largest phase error with root mean square value (RMS) 0.0358 rad, whereas green and blue channels have smaller values 0.0194 and 0.0148 rad respectively

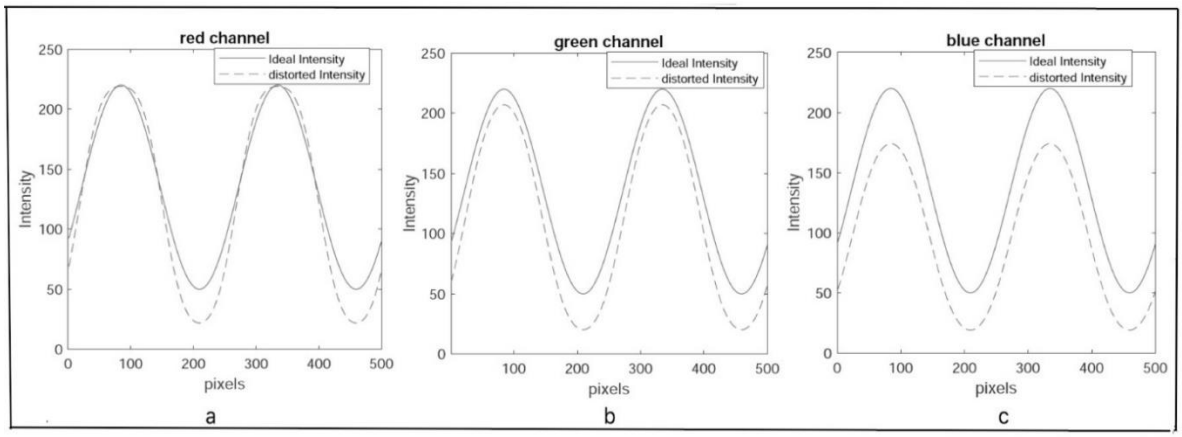

Fig. 7. Ideal and distorted intensity for red (a), green (b), and blue (c) channels respectively.

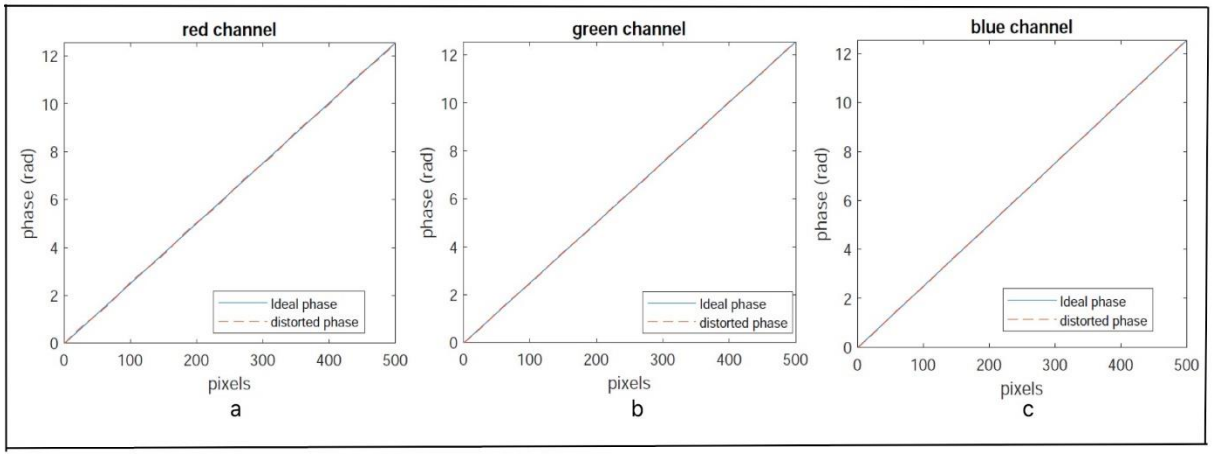

Fig. 8. Ideal and distorted phase for red (a), green (b), and blue (c) channels respectively

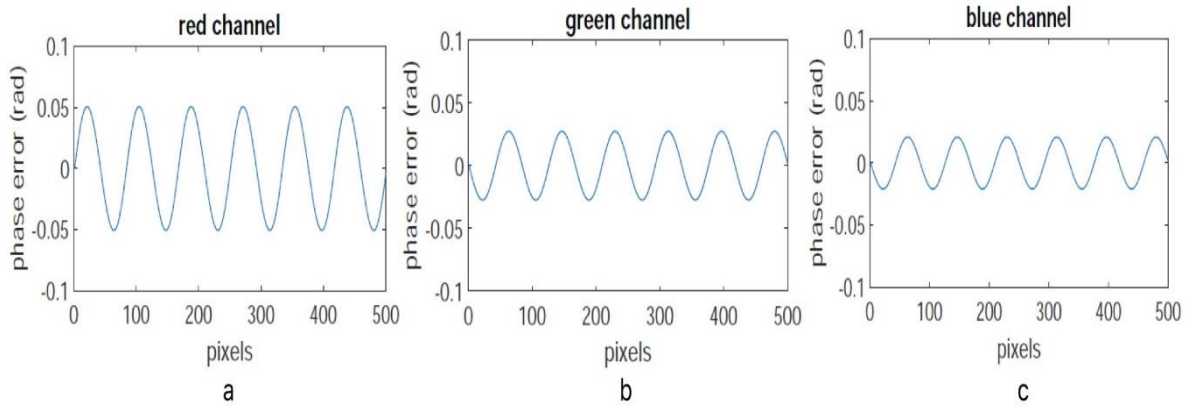

Fig. 9. Phase error using nonlinear gamma effect curve for red (a), green (b), and blue (c) channels respectively.

Fig. 10 shows the actual phase error of red, green, and blue channels. Green channel has the smallest phase error with root mean square (RMS) value 0.0.221 rad, while red and blue channels have RMS values 0.0310 and 0.0334 rad respectively, without any compensation for the phase error in the phase domain. The system has small phase error value comparing with other systems using other types of projectors such as DLP devices where the phase error reaches the value 0.116 rad without nonlinear gamma correction [27]. Since green channel has the smallest phase error value, green patterns are used in the following sections of this study.

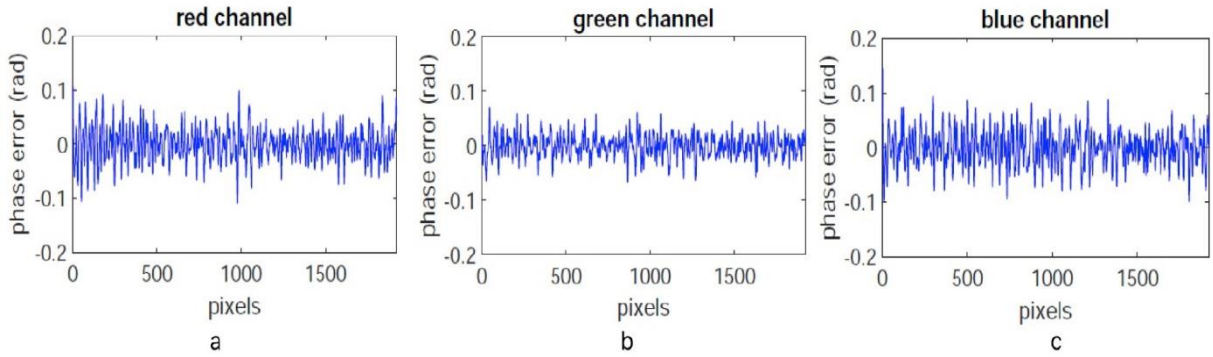

Fig. 10. Actual phase error for red (a), green (b), and blue (c) channels respectively, at 500th row of unwrapped phase map.

4.3. Focus-free projection and depth of field

The focus-free projection of the laser projector is tested at four distances 500, 1000, 1500, and 1725 mm. Fig. 11 shows the profile of 500th row of binary pattern image at 500 mm (a), 1000 mm (b), 1500 mm (c) and 1725 mm (d) respectively. It looks like square wave at all distances proving that the laser projector introduces a focus-free projection at distance up to 1725 mm. RMS value of phase error is calculated at each different projecting distances and listed in Table 1.

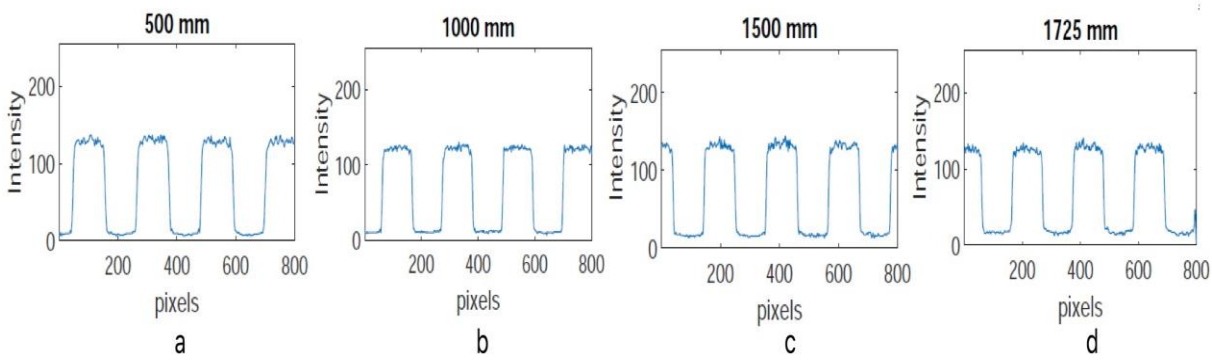

Fig. 11. Profile of 500th row of binary pattern at 500 mm (a), 1000 mm (b), 1500 mm (c) and 1725 mm (d) respectively.

Table 1 illustrates that phase error increases from 0.0212 rad at 500 mm to 0.0331 rad at 1725 mm. Also, phase error at distance between 500 and 800 mm has low and nearly constant phase error, so this range is chosen to realize the large depth of field of the system.

Projecting distance (mm)	Phase error (rad)	Projecting distance (mm)	Phase error (rad)
500	0.0212	1000	0.0257
600	0.0220	1500	0.0317
700	0.0223	1725	0.0331
800	0.0232	----	--------

Fig. 12 (a, b, c, and d) illustrates the profile of 500th row of fringe images at distance 800, 700, 600, and 500 mm where binary projected patterns look like square wave at all distances, and the intensity increases as the reference surface is moved towards the system (camera and projector) proving that the system has large depth of field. This behavior is opposite to the traditional FPP systems where the binary patterns are defocused at different degrees by changing the distance and its profile tends to be sinusoidal wave [19].

On the other hand, when sinusoidal fringe patterns are projected on the reference surface at distances (800, 700, 600, 500) mm, the patterns are not blurred, contrariwise the intensity curve is getting more sharpness as the distance between the reference surface and the system is decreased as shown in Fig. 12 (e, f, g, and h).

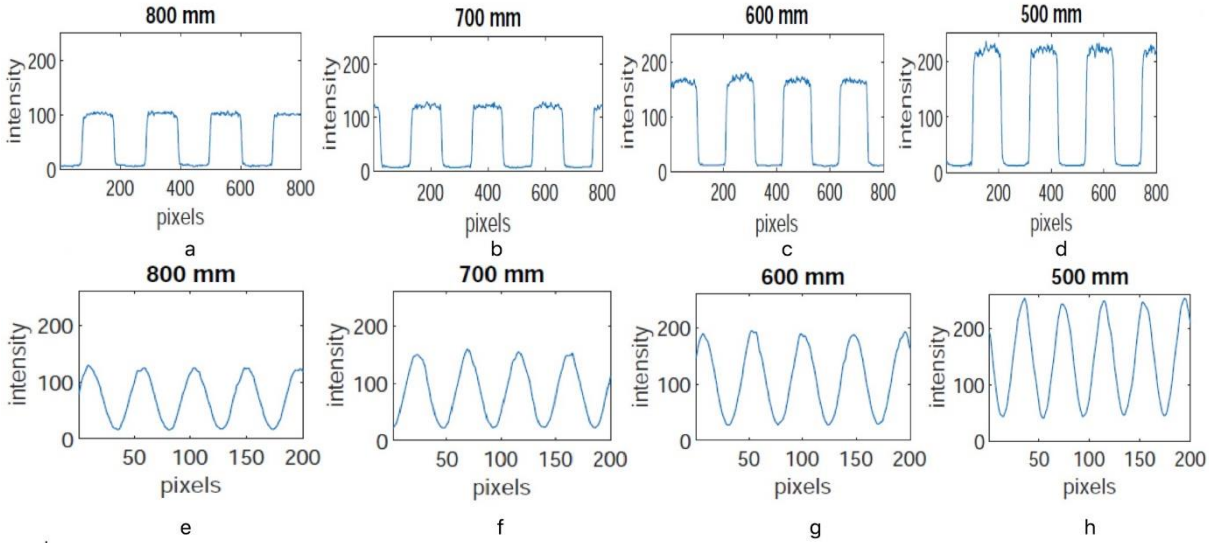

Fig. 12. Cross-section of 500th row of binary fringe images at 800 mm (a), 700 mm (b), 600 mm (c) and 500 mm (d); and sinusoidal fringe images at 800 mm (e), 700 mm (f), 600 mm (g) and 500 mm (h) respectively.

If the reference surface is moved a distance less than 500 mm the camera sensor starts to saturate resulting in losing of the sinusoidal form of the patterns causing serious error in phase calculations. Also, the camera lens tends to be unfocused causing blurring of the captured images and losing the surface details when an object is measured. So, the main parameters that limit the working distance are the aperture of the camera lens and saturation of camera sensor. Fig. 13 shows phase error of 500th row of the unwrapped phase map after removing gross slope at 800, 700, 600, and 500 mm. RMS values are 0.0232, 0.0224, 0.0220 and 0.0212 rad at 800, 700, 600, and 500 mm respectively, which is nearly constant at the mentioned distances resulting in working distance equals to 300 mm with low constant phase error.

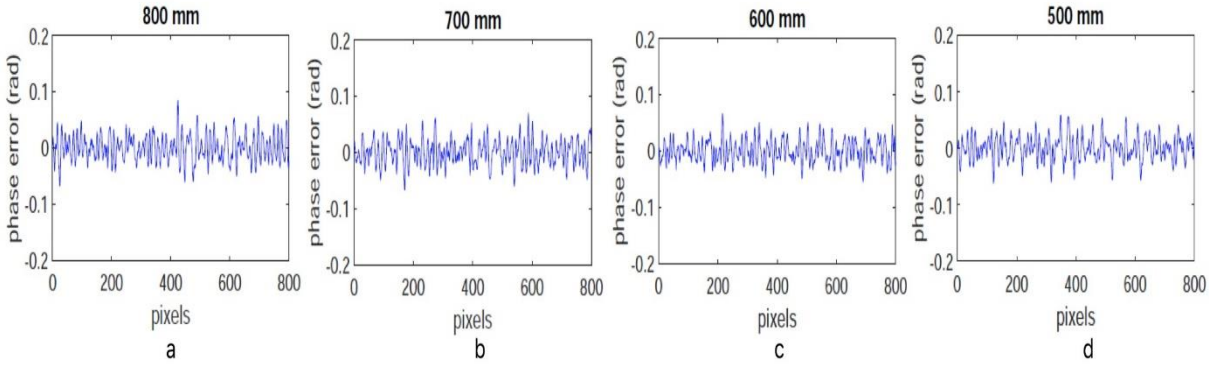

Fig. 13. Phase error at 800 mm (a), 700 mm (b), 600 mm (c) and 500 mm (d) respectively.

4.4. Practical example

As a practical example to ensure the efficiency of the system to have large depth of field and measurement space of the system, a cylindrical object is imaged at four different positions (800, 700, 600 and 500) mm. Fig. 14 shows the phase shift map due to the object at 800, 700, 600, and 500 mm. The differences in x and y directions of phase maps, shown in Fig. 14 (a, b, c, and d) are caused by the change of field of view of the camera at each distance. The differences in z direction arise from the change of value of the phase shift caused by the object height when fringe patterns of the same period are used at different distances. The phase maps are clear with low level of irregularities as an indication of the small phase error values at all distances. This demonstrates the large depth of field and the large working range of the system.

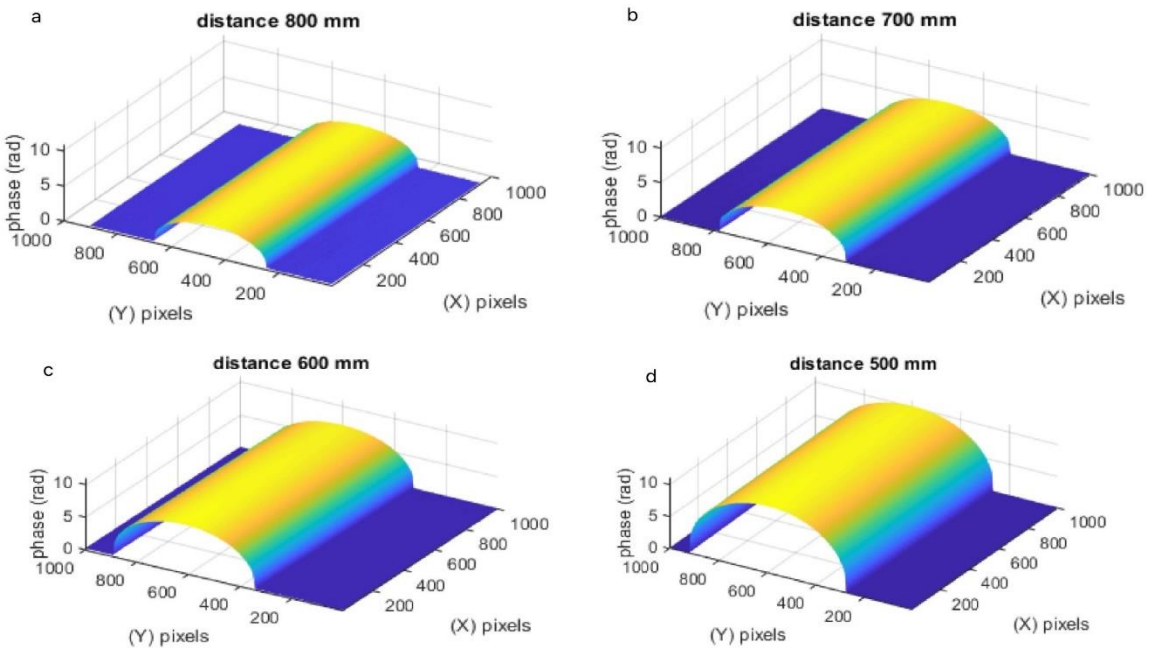

Fig. 14. Phase shift maps of cylindrical surface at 800 mm (a), 700 mm (b), 600 mm (c), and 500 mm (d) respectively

5. Conclusion

- This paper introduces a new simple fringe projection Profilometry (FPP) system using a new type of projectors. It is a laser projector that has the advantage of focus-free projection. Nonlinear gamma effect curve has been studied for red, green, and blue colour channels. Green channel has the smallest phase error with RMS value equals to 0.0221 rad without any compensation for the phase error in the phase domain, while red and blue channels have RMS values 0.0310 and 0.0334 rad respectively. So, the green patterns are used in other sections of this work.
- The laser projector introduces a focus-free projection at distance up to 1725 mm with phase error increases from 0.0212 rad at 500 mm to 0.0331 rad at 1725 mm. Also, phase error at distance between 500 and 800 mm has low and nearly constant phase error, so this range is chosen to realize the large depth of field of the system.
- The system has depth of field (DOF) and working distance up to 300 mm within the distance from 800 to 500 mm with small and nearly constant phase error with RMS value does not exceed 0.0232 rad without any compensation for the phase error in the phase domain. The system has small phase error value comparing with other systems using other types of projectors such as DLP devices where the phase error reaches the value 0.116 rad without nonlinear gamma correction.
- The large depth of field and working range of the system are demonstrated by phase map calculation of cylindrical surface at four different positions 800, 700, 600 and 500 mm. The phase maps are clear with low level of irregularities as an indication of the small phase error values at all distances. This demonstrates the large depth of field and the large working range of the system

Acknowledgement

The authors would like to thank National Institute for standards (NIS) for financial support. Thanks to our colleagues in Surface and Engineering Metrology Lab., Length and Precision Engineering Division at (NIS) for their technical support.

References

[1] Yu J., and Da F. Calibration refinement for a fringe projection profilometry system based on surface homography, Optics and Lasers in Engineering, 140, 106525 (2021).

[2] Yin Y., Mao J., Meng X., Yang X., Wu K., Xi J. and Sun B. A two-step phase-shifting algorithm dedicated to fringe projection profilometry, Optics and Lasers in Engineering, 137, 106372 (2021).

[3] He X. and Qian K. A comparative study on temporal phase unwrapping methods in high- speed fringe projection profilometry, Optics and Lasers in Engineering, 142, 106613 (2021).

[4] Gorthi S. S. and Rastogi P. Fringe Projection Techniques: Whither we are?, Optics and Lasers in Engineering, 48 (2), 133-140 (2010).

[5] Li B. and Zhang S. Microscopic structured light 3D profilometry: Binary defocusing technique vs. sinusoidal fringe projection, Optics and Lasers in Engineering, 96, 117–123 (2017).

[6] Zhang J., Luo B., Su X., Li L., Li B., Zhang S. and Wang Y. A convenient 3D reconstruction model based on parallel-axis structured light system, Optics and Lasers in Engineering, 138, 106366 (2021).

[7] Sicardi-Segade A., Estrada J.C., Martínez-García A. and Garnica G. On axis fringe projection: A new method for shape measurement, Optics and Lasers in Engineering, 69,29–34 (2015).

[8] Feng S., Zuo C., Zhang L., Tao T, Hu Y., Yin W., Qian J. and Qian Chen. Calibration of fringe projection profilometry: A comparative review. Optics and Lasers in Engineering, 143, 106622 (2021).

[9] Yao P., Gai S. and Da F. Coding-Net: A multi-purpose neural network for Fringe Projection Profilometry, Optics Communications, 489, 126887 (2021).

[10] Muhd Ibnur Rashad B. Zainal A., Jie G. L. M., Wee M., Lai T., Fu Y. and Shang H.M. A Simple Laboratory Set-up for The Fringe-Projection Method, Seventh International Conference on Education and Training in Optics and Photonics, Proceedings of SPIE Vol. (4588), (2002).

[11] Spagnolo G. S. and Ambrosini D. Diffractive optical element-based profilometer for surface inspection, Optics and Lasers in Engineering, 40 (1), 44–52 (2001).

[12] Pennington T. L., Xiao H., May R. and Wang A. Miniaturized 3-D surface profilometer using a fiber optic coupler, Optics & Laser Technology, 33, 313–320 (2001).

[13] Li E. B., Peng X., Xi J., Chicharo J. F., Yao J. Q. and Zhang D. W. Multi-frequency and multiple phase-shift sinusoidal fringe projection for 3D profilometry, Optics Express 13, 1561 (2005).

[14] Ratnam M., Saxena M. and Gorthi S. S. Circular fringe projection technique for out-of-surface deformation measurements, Optics and Lasers in Engineering, 121, 369–376 (2019).

[15] [15] Villa J., Araiza M., Alaniz D., Ivanov R. and Ortiz M. Transformation of phase to (x,y,z)- coordinates for the calibration of a fringe projection profilometer, Optics and Lasers in Engineering, 50, 256–261 (2012).

[16] García-Isáis C.A. and Ochoa A. N. One shot profilometry using a composite fringe pattern, Optics and Lasers in Engineering, 53, 25–30 (2014)

[17] Kanga X., Li T., Sia B., Li J. and Yang L. A novel calibration method for arbitrary fringe projection profilometry system, Optik, 148, 227–237 (2017).

[18] Zhong M., Hu X., Chen F., Xiao C., Peng D. and Zhang S. Autofocusing method for a digital fringe projection system with dual projectors, Optics Express, (28), 12609 (2020).

[19] Lei S. and Zhang S. Digital sinusoidal fringe pattern generation: Defocusing binary patterns VS focusing sinusoidal patterns, Optics and Lasers in Engineering, 48, 561–569 (2010).

[20] Zhang Z. H. Review of single-shot 3D shape measurement by phase calculation-based fringe projection techniques, Optics and Lasers in Engineering, 50, 1097–1106 (2012).

[21] Liu Y., Fu Y., Zhuan Y., Zhong K. and Guan B. High dynamic range real-time 3D measurement based on Fourier transform profilometry, Optics & Laser Technology, 138, 106833 (2021).

[22] Zhang Z., Jing Z., Wanga Z. and Kuang D. Comparison of Fourier transform, windowed Fourier transform, and wavelet transform methods for phase calculation at discontinuities in fringe projection profilometry, Optics and Lasers in Engineering, 50,1152–1160 (2012).

[23] Li H. and Yang C. Two-dimensional multiscale windowed Fourier transform based on two-dimensional wavelet transform for fringe pattern demodulation, Optics & Laser Technology, 43, 72–81 (2011).

[24] Shang W., Liu S., Wang J. and Shao R. Analysis and reduction of error caused by tested object using fringe projection technique with wavelet transform, Optik, 221, 165372 (2020).

[25] Zuo C., Feng S., Huang L., Tao T., Yin W. and Chen Q. Phase shifting algorithms for fringe projection profilometry: A review, Optics and Lasers in Engineering, 109, 23–59 (2018).

[26] Huang T., Li X., Fu Xi., Zhang C., Duan F. and Jiang J. Arbitrary phase shifting method for fiber-optic fringe projection profilometry based on temporal sinusoidal phase modulation, Optics and Lasers in Engineering, 121, 300–306 (2019).

[27] ZHANG S. Comparative study on passive and active projector nonlinear gamma calibration, Applied Optics, 54, 13 (2015).